Conserved nuclear receptors controlling a novel trait target fast-evolving genes expressed in a single cell

Bogdan Sieriebriennikov[1,2], Shuai Sun[1], James W. Lightfoot[1], Hanh Witte[1], Eduardo Moreno[1], Christian Rödelsperger[1], Ralf J. Sommer[1]*

[1] Department for Integrative Evolutionary Biology, Max Planck Institute for Developmental Biology, Tübingen 72076, Germany

[2] Current affiliation: Department of Biology, New York University, New York, NY 10003, USA

* corresponding author, ralf.sommer@tuebingen.mpg.de

Abstract

Environment shapes development through a phenomenon called developmental plasticity. Deciphering its genetic basis has implications for understanding evolution and adaptation to novel environments, yet molecular studies are scarce. Here, we expanded the gene regulatory network controlling predatory *vs.* non-predatory morphology in the nematode *Pristionchus pacificus*. First, we isolated a mutant in the nuclear hormone receptor *nhr-1* with a previously unseen phenotypic effect. It disrupts mouth-form determination and results in animals combining features of both wild-type morphs. Further, we identified common targets of NHR-1 and the previously identified nuclear hormone receptor NHR-40 through transcriptomics. Unlike their highly conserved regulators, the target genes have no orthologs in *Caenorhabditis elegans* and likely result from lineage-specific expansions. An array of transcriptional reporters revealed co-expression of all tested targets in the same pharyngeal gland cell. The morphological remodeling of this cell accompanied the evolution of teeth and predation, linking rapid gene turnover with morphological innovations.

Keywords

Developmental plasticity, nuclear hormone receptors, *Pristionchus pacificus*, gene regulatory networks, switch genes, Astacins, evolutionary novelty.

Introduction

Developmental plasticity is the ability to generate different phenotypes in response to environmental input[1]. As a result, even genetically identical individuals may develop distinct phenotypes, the most extreme example being castes in social insects[2]. Developmental plasticity is attracting considerable attention in the context of adaptation to climate change[3–6] and as a facilitator of evolutionary novelty[7–11]. However, the role of plasticity in evolution has been contentious[6,12] because the genetic and epigenetic underpinnings of plastic traits have long remained elusive. Nonetheless, recent studies have begun to elucidate associated molecular mechanisms in insects and nematodes[13–16]. Ultimately, the identification of gene regulatory networks (GRN) controlling plasticity will provide an understanding of development in novel environments and enable testing theories about the long-term evolutionary significance of plasticity.

The free-living nematode *Pristionchus pacificus* has recently been established as a model to study plasticity[13]. These worms can develop two alternative mouth forms, called eurystomatous (Eu) and stenostomatous (St) mouth forms, respectively. Eu morphs have a wide buccal cavity and two large opposed teeth enabling predation on other nematodes, while St morphs have a narrow buccal cavity and one tooth limiting their diet to microbial sources[17,18] (Fig. 1A-C, SFig. 1A). The wild-type *P. pacificus* strain PS312 preferentially forms Eu morphs in standard culture conditions on agar plates, but becomes predominantly St in liquid culture[19]. Additionally, nematode-derived modular metabolites excreted by adult animals induce the predatory Eu morph[20,21]. A forward genetic screen identified the sulfatase gene *eud-1* as a developmental switch confirming long-standing predictions that plastic traits are regulated by binary switches[18]. Subsequent studies implicated several other enzyme-encoding genes, such as *nag-1*, *nag-2*, and *sult-1/seud-1* in regulating mouth-form plasticity[22–25]. Additionally, the chromatin modifier genes *lsy-12* and *mbd-2* influence *eud-1* expression[26]. In contrast, only one transcription factor, the nuclear hormone receptor (NHR) NHR-40, was so far found to regulate mouth-form fate[27], and no downstream targets have been identified (Fig. 1D).

Here, we leveraged the power of suppressor screen genetics to identify the conserved nuclear hormone receptor NHR-1 as a second transcription factor controlling mouth-form development. It differs from *nhr-40* and all the other genes identified to date in that *nhr-1* mutants develop a morphology that combines features of the two morphs, consistent with disrupted mouth-form determination. Furthermore, transcriptomic profiling revealed that NHR-40 and NHR-1 share transcriptional targets, which exhibit functional redundancy and are expressed in a single pharyngeal gland cell, g1D. This cell has undergone extreme morphological remodeling in nematode evolution, which is associated with the emergence of teeth and predatory feeding. Interestingly, *nhr-1* and *nhr-40* are well conserved, whereas all target genes are rapidly evolving and have no orthologs in *C. elegans*. This study enhances the understanding of the GRN regulating mouth-form plasticity, elucidates the evolutionary dynamics of underlying genes and links morphological innovations with rapid gene evolution.

Results and Discussion

Suppressor screen in *nhr-40* identifies another NHR gene regulating mouth-form development

While our previous studies have identified various components involved in the regulation of mouth form plasticity, most of these genes are expressed in neurons responsible for environmental sensing and we are yet to find factors acting in the tissues forming the mouth structure. Therefore, we looked for more downstream factors by conducting a suppressor screen in the mutant background of *nhr-40*. This is the most downstream gene in the current GRN controlling *P. pacificus* mouth-form plasticity and it encodes a transcription factor[27]. We mutagenized *nhr-40(tu505)* worms, which are all-Eu, and isolated one allele, *tu515*, that had a no-Eu phenotype (Fig 1E, Table 1). The phenotype was fully penetrant, both in the presence of *nhr-40(tu505)* and after outcrossing, *i.e.* Eu animals were never observed under any culture condition. Thus, *tu515* represents a novel factor influencing the mouth-form ratio. Interestingly, however, *tu515* mutants also exhibited a non-canonical mouth morphology (Fig. 1A, SFig. 1A, SFig. 3). In contrast to all previously isolated mutants, which either display altered mouth-form frequencies or an aberrant morphology, *tu515* individuals develop a morphology that combines normal features of the two morphs with no apparent dimorphism. Specifically, *tu515* mutants closely resemble the St morph in that they have a flattened dorsal tooth, lack a fully developed right ventrosublateral tooth, and the anterior tip of the promesostegostom aligns with the anterior tip of the gymnostom plate. However, the width of the mouth and the curvature of the dorsal tooth appear intermediate between Eu and St, and the right ventrosublateral ridge is frequently enlarged and resembles an underdeveloped tooth of the Eu morph (Fig. 1A, SFig. 1A). Therefore, while other known mutants affect mouth-form determination by changing the preferred developmental trajectory, *tu515* is the first mutant that disrupts determination, resulting in non-canonical morphology that resembles the St morph but combines features of both morphs.

105 To map *tu515*, we performed bulk segregant analysis. We examined the list of non-
106 synonymous and nonsense mutations within the candidate region on the X chromosome
107 (SFig. 2B, STable 1) and discovered a non-synonymous mutation in another NHR-encoding
108 gene, *nhr-1*. The substitution changed the sequence of a highly conserved FFRR motif within
109 the DNA recognition helix[28] to FFRW, which may cause the loss of DNA-binding activity. We
110 performed the following experiments to verify that *nhr-1* is the suppressor of *nhr-40(tu505)*.
111 First, we created *nhr-1* mutants using CRISPR/Cas9 by generating frameshift mutations at the
112 beginning of the ligand-binding domain (LBD). The resulting alleles *tu1163* and *tu1164*
113 exhibited a no-Eu phenotype and the same morphological abnormalities as *tu515* (Fig. 1A,
114 SFig. 1A, Table 1). Second, we crossed the *tu1163* and *tu515* mutants and established that
115 *tu1163/tu515* trans-heterozygotes were no-Eu showing that the two mutants do not
116 complement each other (Table 1). Third, we overexpressed the complementary DNA (cDNA)
117 of *nhr-1* driven by the *nhr-1* promoter region in the *nhr-1(tu1163)* mutant background and
118 obtained an almost complete rescue (Table 1). Fourth, we crossed *nhr-1(tu1163)* with *nhr-*
119 *40(tu505)* and observed a highly penetrant no-Eu phenotype in double mutant animals, similar
120 to the phenotype of *tu515 nhr-40(tu505)* mutants (Table 1). Taken together, frameshift alleles
121 of *nhr-1* and the original suppressor allele *tu515* exhibit the same phenotype, do not
122 complement each other, and have identical epistatic interactions with *nhr-40(tu505)*.
123 Therefore, we conclude that *nhr-1* is the suppressor of *nhr-40(tu505)*.
124
125 **Reverse genetic analysis of *nhr-40* results in all-stenostomatous mutants**
126 The available alleles of *nhr-1* and *nhr-40* have different phenotypes with regard to
127 mouth-form frequency and morphology. This is surprising because NHRs often form
128 heterodimers[29], in which case *loss-of-function* phenotypes of interacting partners are identical.
129 Two different hypotheses could explain our observations. First, *nhr-1* and *nhr-40* may indeed
130 have different functions. Second, the three available alleles of *nhr-40* (*tu505, iub6, iub5*), all of
131 which are non-synonymous substitutions outside of the DNA-binding domain (DBD)[27], may
132 represent *gain-of-function* alleles. Our previous analysis had suggested that these alleles are

133 *loss-of-function* based on the phenotype of *nhr-40* overexpression, which resulted in all-St
134 animals[27]. However, we recently realized that in *C. elegans*, overexpression of *Cel-nhr-40* and
135 *loss-of-function* of *Cel-nhr-40* induced by RNAi and a deletion mutation all cause similar
136 developmental defects[30]. This may occur if NHR-40 inhibits its own transcription[31] or if the
137 concatenated coding sequence of the rescue construct acts as a substrate to induce RNAi[30].
138 Therefore, we investigated *nhr-40* in *P. pacificus* further, and generated nonsense alleles
139 using CRISPR/Cas9.

140 We introduced mutations in two different locations in *nhr-40* (Fig. 2A). The alleles
141 *tu1418* and *tu1419* truncate the DBD. The *tu1420* allele contains a frameshift at the beginning
142 of the LBD while leaving the DBD intact. We phenotyped the newly obtained mutants in liquid
143 S-medium, which represses the Eu morph, and on agar plates, which induces it[19]. All
144 frameshift alleles had a completely penetrant all-St phenotype in both culture conditions, which
145 is opposite to the original ethyl methanesulfonate (EMS) alleles (Table 1). The newly obtained
146 *nhr-40* mutants displayed no morphological abnormalities seen in *nhr-1* mutants. Additionally,
147 we created a *null* allele, *tu1423*, which contains a 13 kb deletion or rearrangement of the locus
148 (SFig. 2A). This *null* allele again had a completely penetrant all-St phenotype and showed no
149 morphological abnormalities (Table 1). To eliminate the possibility that the phenotype of the
150 EMS mutants was caused by random mutations outside *nhr-40*, we introduced a nucleotide
151 substitution identical to *iub6* via homology-directed repair (Fig. 2A). Indeed, the two resulting
152 alleles, *tu1421* and *tu1422*, had an all-Eu phenotype, identical to that of *iub6* and other EMS
153 alleles, and opposite to that of the frameshift alleles (Table 1). Thus, frameshift mutations in
154 DBD, LBD, and the deletion/rearrangement of the entire gene have an opposite phenotype to
155 that of the three previously isolated non-synonymous substitutions. We conclude that *tu505,*
156 *iub6, iub5, tu1421* and *tu1422* are *gain-of-function* alleles.
157
158 **NHR-40 and NHR-1 interact post-transcriptionally**
159 In GRNs, transcription factors may activate or repress each other transcriptionally[32–36],
160 or alternatively, they may interact at the post-transcriptional level. The latter includes indirect

interactions, such as independent binding to the same promoters[37], or ligand-mediated interactions[38]. To distinguish if *nhr-1* and *nhr-40* interact at the transcriptional or post-transcriptional level, we analyzed the transcriptomes of wild type, *nhr-1 loss-of-function*, *nhr-40 loss-of-function* and *nhr-40 gain-of-function* mutants at two developmental stages (Fig. 3A). RNA collected from J2-J4 larvae is enriched with transcripts expressed at the time of mouth-form determination, as environmental manipulation during this time window affects morph frequency[39]. RNA collected from J4 larvae and adults is enriched with transcripts expressed at the time of mouth-form differentiation, because cuticularized mouthparts that distinguish the two morphs are believed to be secreted during the J4-adult molt[40]. We found that at both time points, *nhr-40* transcript levels were not affected by *loss-of-function* of *nhr-1*. Similarly, *nhr-1* transcript levels were not affected by *loss-of-function* of *nhr-40*, although they were slightly, but not significantly increased by *nhr-40 gain-of-function* (Fig. 2B). Thus, at the transcriptional level, both *nhr* genes remain unaffected by the *loss-of-function* of the other *nhr* gene. Therefore, NHR-40 and NHR-1 may interact at the post-transcriptional level, although the possibility remains that their transcriptional interaction in specific cells is masked in whole-animal transcriptome data. The lack of linear transcriptional regulation is consistent with different phenotypic effects of *nhr-40* and *nhr-1*.

nhr-40 and _nhr-1_ are expressed at the site of polyphenism

Next, we wanted to determine the expression pattern of *nhr-1* and *nhr-40* and test if they were co-expressed. We took three complementary approaches to establish the expression pattern of *nhr-1*. First, we created transcriptional reporters comprising the presumptive promoter region upstream of the potential start site in the second exon fused with TurboRFP or Venus. The resulting expression pattern was broad with the strongest expression in the head, including both muscle and gland cells of the pharynx, and what may be the hypodermal and arcade cells (Fig. 2D, SFig. 1B). Second, we performed antibody staining against an HA epitope tag in the *nhr-1* rescue line described above. We observed a similar expression pattern that was predictably localized to the nuclei (Fig. 2C). Finally, we used

CRISPR/Cas9 to "knock in" an HA tag in the endogenous *nhr-1* locus at the C-terminus of the coding sequence. Antibody staining against HA revealed a similar expression pattern but with a weaker signal due to the lower number of copies of endogenous DNA (SFig. 1C). Together, these results show that NHR-1 localizes to nuclei of multiple cells in the head region, with strong expression in pharyngeal muscle cells, which presumably secrete structural components of the teeth.

To explore whether NHR-40 and NHR-1 are expressed in overlapping tissues, we created a double reporter line, in which the *nhr-40* promoter is fused to TurboRFP and the *nhr-1* promoter to Venus. We observed a strong and consistent expression of *nhr-40* in the head. Specifically, it localized to the pharyngeal muscle cells and cells whose cell body position is consistent with them being arcade or hypodermal cells (Fig. 2D, SFig. 1D). *nhr-40* and *nhr-1* signals co-localized in a subset of presumptive hypodermal and arcade cells, and in the pharyngeal muscles. In contrast, only *nhr-1* was expressed in the dorsal pharyngeal gland cell g1D (Fig. 2D, SFig. 1D,E). In summary, while the expression of *nhr-40* is more restricted than the expression of *nhr-1*, the two genes display robust co-localization in several cell types.

Suppressor screen in *nhr-1* failed to identify downstream target genes

The experiments described above established that two NHR-type transcription factors control mouth-form plasticity in *P. pacificus*. We speculate that NHR-40 and NHR-1 regulate a set of target genes, which execute the developmental decision and generate alternative phenotypes. To identify such downstream target genes, we performed genetic and transcriptomic analyses. In the first attempt, we conducted two suppressor screens in the *nhr-1(tu1163)* mutant background. In total, we screened approximately four times more gametes than in our first suppressor screen, but we isolated no all-Eu lines. There are three explanations for this result. First, functional *nhr-1* may be essential for the Eu morph. Second, the number of downstream targets may be small, and a considerably larger screen is required to identify them. Third, the downstream targets may be redundant, and multiple genes may

need to be inactivated to change the phenotype. Therefore, we took an alternative approach and identified targets of NHR-40 and NHR-1 through transcriptomic profiling.

Common transcriptional targets of NHR-40 and NHR-1 encode extracellular proteins expressed during mouth-form differentiation

Since NHR-40 and NHR-1 are co-expressed and regulate the same phenotype, we speculate that they regulate a set of common target genes. We analyzed the full list of genes differentially expressed between the wild type and mutant samples from the experiments described above. Given the pleiotropic action of NHR-40 and NHR-1, we applied the following selection criteria. We only retained genes whose transcript levels at either of the two examined time points were simultaneously altered in *nhr-1*, *nhr-40 loss-of-function*, and *nhr-40 gain-of-function* mutants (Fig. 3A). Only 28 genes satisfied this criterion, and their expression changed in the same direction in the *loss-of-function* mutants of *nhr-1* and *nhr-40*. We further retained those genes whose expression changed in one direction in the *loss-of-function* mutants of *nhr-1* and *nhr-40*, and in the opposite direction in the *gain-of-function* mutants of *nhr-40* (Fig. 3A), resulting in a list of 24 genes, provided in Table 2, Interestingly, the expression of 23 of them decreased in the *loss-of-function* mutants (Table 2).

We hypothesized that if the making of cuticularized mouthparts involves these genes, they must encode extracellular proteins, and their expression is likely to be biased towards the time of mouth-form differentiation. To verify the extracellular function of the target proteins, we predicted signal peptides and compared the list of targets with the genome-wide pattern. Indeed, we found that the targets of NHR-40 and NHR-1 are significantly enriched with genes containing signal peptides (Fig. 3B). To examine a potential temporal expression bias, we compared the wild-type transcriptomes at the time of mouth-form determination and mouth-form differentiation. While most genes in the genome (51%) showed uniform expression at the two time points, 23 of the 24 targets of NHR-40 and NHR-1 where more highly expressed at the time of mouth-form differentiation (Fig. 3B). Surprisingly, we also observed a third trend in our data set. While only 12% of all genes in the genome are located on the X chromosome,

15 of the 24 targets of NHR-40 and NHR-1 were X-linked (Fig. 3B). Previously identified genes associated with mouth-form plasticity are frequently situated on the X-chromosome, including both *nhr-40* and *nhr-1*, and additionally the multigene locus comprising *eud-1, nag-1* and *nag-2*. While the exact meaning of this phenomenon remains unclear, the X chromosome in *C. elegans* is enriched with hermaphrodite-biased somatically expressed genes[41]. Accordingly, the incidence of Eu morphs is higher in *P. pacificus* hermaphrodites than in males[39], which may be reflected in the chromosomal distributions of the genes associated with the Eu morph. In summary, the downstream targets of NHR-40 and NHR-1 are enriched with genes that are X-linked, encode extracellular proteins, and are more highly expressed at the time of mouth-form differentiation.

To explore the potential functions of the NHR-40 and NHR-1 targets, we used information about their annotated protein domains. Surprisingly, 12 of the 24 genes contain an Astacin domain (Table 2). Astacins are secreted or membrane-anchored Zinc-dependent endopeptidases, first described in the crayfish *Astacus astacus*[42]. Of the 40 genes present in *C. elegans*, only *dpy-31, nas-6* and *nas-7* have known functions, whereby mutations in these genes result in abnormal cuticle synthesis[43,44]. Another five of the 24 NHR targets encode a CAP (**c**ysteine-rich secretory proteins, **a**ntigen 5, and **p**athogenesis-related 1) domain (Table 2), which is contained in extracellular proteins with diverse functions[45-47], including the proteolytic modification of extracellular matrix[48]. Two genes belong to the glycoside hydrolases family 18 (Table 2), which includes chitinases and chitinase-like proteins[49] that may modify the cuticle, as chitin is the main component of the cuticle in nematodes[50]. Finally, the NHR target list includes an unannotated protein, PPA30108 (Table 2), which contains multiple GGX repeats, where X is F or R. Intriguingly, a similar sequence repeat has been proposed to facilitate the formation of elastic fibers by structural proteins of spider silk[51,52]. Thus, the examination of the coding sequences and domain composition of the targets of NHR-40 and NHR-1 shows that most encode enzymes that may directly modify the cuticle, and one gene encoding what may be an elastic structural protein.

A duodecuple Astacin mutant shows no mouth-form abnormalities

Next, we tested if mutations in the identified genes affected mouth-form frequency or morphology. We therefore performed systematic CRISPR/Cas9 knockout experiments of the 23 genes downregulated in the *loss-of-function* mutants. To compensate for potential redundancy between paralogous genes encoding identical domains, we produced lines in which all such genes are inactivated simultaneously. For example, rather than generating 12 strains with mutations affecting single Astacin-encoding genes, we produced a duodecuple mutant line, in which we sequentially knocked out all 12 genes (Table 1). We phenotyped the mutants both on agar plates and in liquid S-medium. However, we detected no significant change in mouth-form frequencies and no recapitulation of the morphological defects of *nhr-1*. Similarly, we produced a quintuple CAP mutant and double chitinase mutants and observed no change in mouth-form frequency or morphology (Table 1). We speculate that this may be caused by the extreme redundancy in the factors involved. For instance, despite mutagenizing 12 Astacin-encoding genes, there are more than 60 such genes in the genome. Consistent with this, in a phenotypic screen of Astacin genes in *C. elegans*, the majority showed no detectable phenotypes and the function of one, *nas-7*, was only elucidated due to its enhancement of a weakly penetrant allele of *nas-6*[44]. Alternatively, it is also possible that some examined genes function in other tissues unrelated to mouth morphology. Therefore, we next studied the spatial expression of selected downstream target genes.

Downstream targets genes are expressed in the same pharyngeal gland cell

We selected six of the 12 Astacin genes, one chitinase gene, one CAP gene, and the gene bearing similarity to spider silk proteins, and created transcriptional reporters by fusing their promoters with TurboRFP. Remarkably, all reporter lines showed expression in the same single cell, the dorsal pharyngeal gland cell g1D (Fig. 3C). In contrast, we found no expression in the pharyngeal muscles or other expression foci of *nhr-40* and *nhr-1*. Thus, all analyzed targets are co-expressed with *nhr-1* in g1D (Fig. 3C, SFig. 1E). The recent reconstruction of the pharyngeal gland cell system of *P. pacificus*[53] revealed that the cell body of g1D is located

at the posterior end of the pharynx. It sends a long process through the entire pharynx to the anterior tip where it connects, via a short duct in the cuticle, to a channel in the dorsal tooth which opens into the buccal cavity (Fig. 1B, 3C). Importantly, the process of g1D is surrounded by pharyngeal muscle cells which directly underlie the teeth. Therefore, we hypothesize that the enzymes excreted from g1D act on the structural components that are themselves secreted by the pharyngeal muscles.

Expansion of the pharyngeal gland cells is concomitant with the emergence of teeth

The expression of the targets of NHR-40 and NHR-1 in g1D is remarkable, because g1D is the site of a major evolutionary innovation in the family Diplogastridae, to which *P. pacificus* belongs. The pharynx in free-living nematodes of the order Rhabditida and the outgroup[54] family Teratocephalidae is divided into two parts. The anterior part, called the corpus, is muscular, and in some lineages ends with a dilation, called the median bulb. The posterior part, called the postcorpus, is divided into a narrow isthmus and a dilation, called the terminal bulb, which contains muscle cells and three to five gland cells. The terminal bulb contains muscular valves that form a specialized cuticular structure, the grinder, which helps fragment food particles[55] (Fig. 4). Phylogenetic reconstruction indicates that the outgroup Teratocephalidae, and the rhabditid families Cephalobidae and Rhabditidae retained the ancestral character states, whereby they have a grinder, but no teeth[56–58]. In contrast, Diplogastridae have no grinder, but they have concomitantly gained teeth at the base of the family[7,59]. The acquisition of teeth and the loss of the grinder were accompanied by the reduction of the muscle cells in the postcorpus, and an expansion of three gland cells g1D, g1VL, and g1VR, one in each sector of the trilaterally symmetrical pharynx[53,59] (Fig. 4). While the exact role of pharyngeal gland cells in *C. elegans* and other nematodes has remained elusive[55], we speculate that the functional remodeling of g1D, in which the target genes of NHR-40 and NHR-1 are expressed, may be a prerequisite for the formation of teeth and the evolution of predation. Therefore, we investigated the evolutionary dynamics of the identified genes expressed in this cell.

Conserved transcription factors regulate fast-evolving target genes

To investigate if the morphological lineage-specific evolutionary innovation in *P. pacificus* and Diplogastridae is associated with taxonomically restricted genes, we reconstructed the phylogeny of NHR genes and their identified targets. This is an important evolutionary question as recent genomic studies involving deep taxon sampling revealed high evolutionary dynamics of novel gene families in *Pristionchus*, with only one third of all genes having 1:1 orthologs between *P. pacificus* and *C. elegans*[60,61]. First, we reconstructed the phylogeny of NHR genes. We identified similar numbers of NHR genes in the genomes of *P. pacificus* and *C. elegans* - 254 and 266 genes, respectively. In the phylogenetic tree (Fig. 5A), most clades contained genes from predominantly or exclusively one of the two species. These genes likely result from lineage-specific duplications and losses, a phenomenon commonly seen in nematode gene families[62]. *nhr-40* and *nhr-1*, however, belonged to one of the few clades that contained a mixture of genes from both species, with many genes displaying a 1:1 orthology relationship. Indeed, the *P. pacificus* and *C. elegans* copies of *nhr-40* and *nhr-1* showed 1:1 orthology with 100% bootstrap support (Fig. 5A). Importantly, *nhr-40* and *nhr-1* are also extremely closely related to each other (Fig. 5A). Thus, in the overall context of NHR evolution, *nhr-40* and *nhr-1* are closely related duplicates that have been conserved since the divergence of *P. pacificus* and *C. elegans*.

The conservation of *nhr-40* and *nhr-1* is in stark contrast to the evolutionary history of their downstream targets. To reconstruct the phylogenies of the Astacin, CAP and chitinase genes (Fig. 5B-D), we used functional domains rather than complete genes to facilitate the alignment of genes with different domain architectures. Similar to the case of NHRs, all three gene families exhibit strong signatures of lineage-specific expansions. Furthermore, all target genes containing Astacin, CAP and chitinase domains belonged to such lineage-specific clades (Fig. 5B-D). These findings suggest that the targets of NHR-40 and NHR-1 undergo rapid turnover. This is further supported by the phylogeny of CAP genes within the genus *Pristionchus*. Specifically, the five targets identified in *P. pacificus* clustered separately from the homologs in the early branching species *P. fissidentatus* with 94% bootstrap support (Fig.

5E). Thus, two conserved NHRs target rapidly evolving downstream genes of multiple gene families. We speculate that the striking co-expression of the target genes results from an ancient regulatory linkage between the NHRs and the promoters of the ancestral target genes. Such divergent evolutionary dynamics of transcription factors and their downstream targets might represent general features of GRNs.

Conclusions

In this study, we expanded the GRN controlling predatory *vs.* non-predatory plasticity in *P. pacificus*, thereby enhancing the molecular understanding of plasticity. We uncovered novel genetic factors and genomic features at two regulatory levels, which allowed linking rapid gene evolution with morphological innovations associated with plasticity. First, we identified a mutation in the nuclear receptor gene *nhr-1*, which disrupts mouth-form determination. Most previously identified genes, such as *eud-1* or *sult-1/seud-1*, influence the determination process by affecting the preferred developmental trajectory, but the resulting morphology exhibits no observable differences to the corresponding wild-type morphology[18,23,24]. On the other hand, interfering with heat shock protein activity, including a mutation in *daf-21*/Hsp90, produces aberrant morphologies while maintaining the dimorphism[63]. In contrast to both classes of genetic interventions, mutations in *nhr-1* lead to a morphology that combines features of normal Eu and St morphs, with no apparent dimorphism. Therefore, we speculate that NHR-1 is required for mouth-form determination and the specification of both morphs. On the contrary, we identified that *gain-* and *loss-of-function* mutations in *nhr-40* result in all-Eu and all-St phenotypes, respectively, reminiscent of the role of *daf-12*, another *nhr* gene, in controlling dauer plasticity in *C. elegans*[64]. Different phenotypic effects of *nhr-1* and *nhr-40* are also consistent with the lack of evidence of transcriptional regulation of one factor by the other. Except for DAF-12 in *C. elegans*, no single nematode NHR has been de-orphanized. Therefore, the identification of the potential ligands of NHR-1 and NHR-40 may reveal additional layers of regulation and elucidate their cross-talk. Indeed, recent studies suggested that cytosolic sulfotransferases, including *sult-1/seud-1* in *P. pacificus* and its homolog *ssu-1* in *C. elegans,* may regulate NHRs by modifying their ligands[23,24,65].

Second, the transcriptomic analysis of *nhr-1* and *nhr-40* mutants revealed an unexpectedly small number of downstream targets. While cell-specific signals may be masked in whole-animal transcriptome data, and our selection criteria excluded genes affected by the

389 *gain-of-function* of *nhr-40* in other ways than by exhibiting increased transcript levels, having
390 a small list of target genes enabled a systematic analysis of their function and expression.
391 Both the absence of phenotypes in duodecuple and quintuple mutants, and the restricted
392 expression of all tested genes in the same cell g1D are compatible with extreme redundancy.
393 Such redundancy might result from features of genome evolution that are common to
394 nematodes and other animals. Studies over the last decade revealed that nematode genomes
395 are gene-rich and exhibit high rates of gene birth and death[60,66,67]. In particular, enzyme-
396 encoding genes are subject to high evolutionary dynamics[62]. Therefore, the position of genes
397 in GRNs may determine the speed and direction of their evolution. Consistent with this idea,
398 many genes encoding proteins of signal transduction and their terminal transcription factors
399 are highly conserved across animals[68–70]. In this study, we complement this knowledge by
400 showing that the downstream targets of conserved transcription factors are indeed fast
401 evolving genes. Importantly, their expression focus, the g1D cell, also underwent a major
402 evolutionary change, whereby its structural and functional remodeling accompanied the
403 emergence of teeth in the family Diplogastridae. Thus, our study demonstrates that fast-
404 evolving genes are expressed in a fast-evolving cell, linking morphological innovations with
405 rapid gene evolution.

Methods

Maintenance of worm cultures and genetic crosses

Stock cultures of all strains used in this study were reared at room temperature (20-25°C) on nematode growth medium (NGM) (1.7% agar, 2.5 g/L tryptone, 3 g/L NaCl, 1 mM $CaCl_2$, 1 mM $MgSO_4$, 5 mg/L cholesterol, 25 mM KPO_4 buffer at pH 6.0) in 6 cm Petri dishes, as outlined in the *C. elegans* maintenance protocol[71]. *Escherichia coli* OP50 was used as food source. Bacteria were grown overnight at 37°C in L Broth (10 g/L tryptone, 5 g/L yeast extract, 5 g/L NaCl, pH adjusted to 7.0), and 400 µL of the overnight culture was pipetted on NGM agar plates and left for several days at room temperature to grow bacterial lawns. *P. pacificus* were passed on these lawns and propagated by passing various numbers of mixed developmental stages. To cross worms, agar plates were spotted with 10 µL of the *E. coli* culture, and five to six males and one or two hermaphrodites were transferred to the plate and allowed to mate. Males were removed after two days of mating.

Mouth form phenotyping

We phenotyped worms in two culture conditions. Rearing *P. pacificus* on solid NGM induces the Eu morph and facilitates identification of Eu-deficient (all-St) phenotypes. Conversely, growing worms in liquid S-medium (5.85 g/L NaCl, 1 g/L K_2HPO_4, 6 g/L KH_2PO_4, 5 mg/L cholesterol, 3 mM $CaCl_2$, 3 mM $MgSO_4$, 18.6 mg/L disodium EDTA, 6.9 mg/L $FeSO_4$•$7H_2O$, 2 mg/L $MnCl_2$•$4H_2O$, 2.9 mg/L $ZnSO_4$•$7H_2O$, 0.25 mg/L $CuSO_4$•$5H_2O$ and 10 mM Potassium citrate buffer at pH 6.0) represses the Eu morph and facilitates identification of Eu-constitutive (all-Eu) phenotypes[19,71]. As food source, S-medium contained *E. coli* OP50 in the amount corresponding to 100 mL of an overnight culture with OD_{600} 0.5 per 10 mL of medium. We started phenotyping by isolating eggs from stock culture plates, which contained large numbers of gravid hermaphrodites and eggs deposited on the agar surface[71]. To isolate eggs, we washed worms and eggs from plates with water, and incubated them in a mixture of 0.5 M NaOH and household bleach at 1:5 final dilution for 10 min with regular vortexing to

disintegrate vermiform stages. Remaining eggs were pelleted at 1,300 g for 30 sec, washed with 5 mL of water, pelleted again, resuspended in water and pipetted on agar plates or into S-medium. Agar plates were left at room temperature (20-25°C) for 3-5 days and 25 mL Erlenmeyer flasks with liquid medium were shaken at 22°C, 180 rpm for 4-6 days. Adult hermaphrodites were immobilized on 5% Noble Agar pads with 0.3% NaN_3 added as an anesthetic, and examined using differential interference contrast (DIC) microscopy. Animals that had a large right ventrosublateral tooth, curved dorsal tooth, and the anterior tip of the promesostegostom posterior to the anterior tip of the gymnostom plate were classified as Eu morphs. Animals that did not exhibit these three characters simultaneously were classified as St morphs, although there was a distinction between the morphology of *nhr-1* mutants and of other all-St mutants (SFig. 1A).

Geometric morphometric analysis

We reused the published[63] landmark data for the wild-type strain RS2333 and the *daf-21(tu519)* mutant. We complemented this data set with newly collected data for the *nhr-1(tu1163)* mutant, whereby we imaged young adults mounted on microscope slides on 5% Noble agar pads containing 0.3% NaN_3 as an anesthetic. Only individuals with their right body side facing upwards were imaged. We took stack images of the anterior tip of the head, and recorded X and Y coordinates of 20 landmarks identical to the ones used in the previous study[63] using FIJI[72]. Procrustes alignment and PCA were done in R (ver. 3.4.4)[73] using geomorph package [74].

CRISPR/Cas9 mutagenesis

We followed the previously published protocol for *P. pacificus*[75] with subsequently introduced modifications[76]. All target-specific CRISPR RNAs (crRNAs) were designed to target 20 bp upstream of the protospacer adjacent motifs (PAMs). We purchased crRNAs and universal trans-activating CRISPR RNA (tracrRNA) from Integrated DNA Technologies (Alt-R product line). 10 µL of the 100 uM stock of crRNA was combined with 10 µL of the 100 uM

stock of tracrRNA, denatured at 95°C for 5 min, and allowed to cool down to room temperature and anneal. The hybridization product was combined with Cas9 protein (purchased from New England Biolabs or Integrated DNA Technologies) and incubated at room temperature for 5 min. The mix was diluted with Tris-EDTA buffer to a final concentration of 18.1 µM for the RNA hybrid and 2.5 µM for Cas9. When site-directed mutations were introduced via homology-directed repair, a ssDNA oligo template designed on the same strand as the gRNA was included in the mix at a final concentration of 4 µM. The diluted mixture was injected in the gonad rachis of approximately one day old adult hermaphrodites. Eggs laid by injected animals within a 12-16 h period post injection were recovered, and the F1 progeny were singled out upon reaching maturity. After F1 animals have laid eggs, they were placed in 10 µL of single worm lysis buffer (10 mM Tris-HCl at pH 8.3, 50 mM KCl, 2.5 mM $MgCl_2$, 0.45% NP-40, 0.45% Tween 20, 120 µg/ml Proteinase K), frozen and thawed once, and incubated in a thermocycler at 65°C for 1 h, followed by heat deactivation of the proteinase at 95°C for 10 min. The resulting lysate was used as a template in subsequent PCR steps. Where possible, molecular lesions at the crRNA target sites were detected by melting curve analysis on a LightCycler 480 Instrument II (Roche) of PCR amplicons obtained using LightCycler 480 High Resolution Melting Master (Roche). Presence of mutations in candidate amplicons was further verified by Sanger sequencing. Alternatively, PCR was done using Taq PCR Master Mix (Qiagen) and all the F1 were Sanger sequenced. To detect large rearrangements, we conducted whole genome re-sequencing of lines for which no PCR amplicon containing the crRNA target site could be obtained. For most such lines, we extracted genomic DNA using GenElute Mammalian Genomic DNA Miniprep Kit (Merck), whereby we modified the tissue digestion step by raising the Proteinase K concentration to 2 mg/mL, and prepared next-generation sequencing (NGS) libraries using Nextera DNA Flex Library Prep Kit (Illumina). For the *nhr-40* null mutant line, we followed a recently introduced cost-effective alternative procedure[77] with several modifications. Single worms were placed in 10 µL water, and frozen and thawed 3 times in liquid nitrogen. Then, we added 10 µL 2x single worm lysis buffer (20 mM Tris-HCl at pH 8.3, 100 mM KCl, 5 mM $MgCl_2$, 0.9% NP-40, 0.9% Tween 20, 240 µg/ml Proteinase K)

and incubated the tubes in a thermocycler at 65°C for 1 h. After a clean-up using HighPrep beads (MagBio Genomics), DNA was eluted in 7 µL Tris buffer at pH 8.0. Then, 100 pg of DNA was diluted with water to the total volume of 9 µL, mixed with 2 µL 5X TAPS-DMF buffer (50 mM TAPS at pH 8.5, 25 mM $MgCl_2$, 50% DMF) and 1 µL Tn5 transposase from Nextera DNA Library Prep Kit (Illumina) diluted beforehand 1:25 in dialysis buffer (100 mM HEPES at pH 7.2, 0.2 M NaCl, 0.2 mM EDTA, 0.2% Triton X-100, 20% glycerol). The mixture was incubated for 14 min at 55°C. Tagmented DNA was amplified using Q5 HotStart High-Fidelity DNA Polymerase (New England Biolabs) for 14 cycles, whereby adapters and indices were added as primer overhangs, and size-selected for 250–550 bp fragments using HighPrep beads (MagBio Genomics). NGS libraries prepared using both methods were sequenced in a paired-end run of a HiSeq 3000 machine (Illumina). Reads were mapped to the El Paco assembly of the *P. pacificus* genome[78] using Bowtie 2 (ver. 2.3.4.1)[79]. We visually inspected read coverage in the loci of interest using IGV[80] to identify the precise regions in which coverage was close to zero.

EMS mutagenesis

To induce heritable mutations in *P. pacificus*, we incubated a mixture of J4 larvae and young adults in M9 buffer (3 g/L KH_2PO_4, 6 g/L Na_2HPO_4, 5 g/L NaCl, 1 mM $MgSO_4$) with 47 mM ethyl methanesulfonate (EMS) for 4 h[81]. Subsequently, the worms were allowed to recover on agar plates with bacteria (see above), and 40-120 actively moving J4 larvae were singled out. After the animals have laid approximately 20 eggs, they were killed, and F1 progeny were allowed to develop and reach maturity. F1 animals (which contained heterozygous mutants) were then singled out, and F2 progeny (which contained a mixture of genotypes, including homozygous mutants) were allowed to develop until adulthood. In each F1 plate, we determined the mouth form in 5-10 F2 individuals using Discovery V20 stereomicroscope (Zeiss). If at least one individual appeared to have a mouth form different from that of the background strain, such an animal was transferred to a fresh plate and its progeny was screened again using DIC until we gained confidence that a homozygous line was isolated. In

518 the screen for suppressors of *nhr-40*, we mutagenized *nhr-40(tu505)* worms, which are all-Eu,
519 screened approximately 1,000 F1 plates, and isolated one no-Eu allele, *tu515*. In an attempt
520 to identify further downstream target genes, we conducted two suppressor screens in the *nhr-*
521 *1(tu1163)* mutant background and screened approximately 3,800 F1 plates in total, but found
522 no Eu individuals.
523
524 **Mapping of tu515**
525 We crossed the *tu515* mutant, produced in the background of the RS2333 strain (a
526 derivative of the PS312 strain), to a highly-Eu wild type strain PS1843. The resulting males
527 were crossed to a strain RS2089, which is a derivative of PS1843 containing a morphological
528 marker mutation causing the Dumpy phenotype. The progeny were allowed to segregate and
529 100 no-Eu lines were established. Four individuals from each line were pooled and genomic
530 DNA was extracted from the pool using the MasterPure Complete DNA and RNA Purification
531 Kit (Epicentre). Additionally, genomic DNA was extracted from the *tu515* line. NGS libraries
532 were prepared using Low Input Library Prep kit (Clontech) and sequenced on Illumina
533 HiSeq3000. Raw Illumina reads of the *tu515* mutant and of a mapping panel were aligned to
534 the El Paco assembly of the *P. pacificus* genome (strain PS312)[78] by the aln and sampe
535 programs of the BWA software package (ver. 0.7.17-r1188)[82]. Initial mutations were called
536 with the samtools (ver. 1.7) mpileup command[83]. The same program was used to measure
537 PS312 allele frequencies in the mapping panel at variant positions with regard to whole
538 genome sequencing data of the PS1843 strain[78]. SFig. 2B shows that large regions between
539 the positions 5 Mb and 16 Mb of the *P. pacificus* chromosome X exhibit high frequency of the
540 PS312 alleles (the mutant background) in the mapping panel. In total, 28 non-
541 synonymous/nonsense mutations (STable 1) in annotated genes (El Paco gene annotations
542 v1, Wormbase release WS268) were identified in the candidate interval by a previously
543 described custom variant classification software[84].
544
545

546 **Transgenesis**

547 To identify putative promoter regions, which included 5' untranslated regions (UTR)
548 and may have included the beginning of coding sequences, we manually re-annotated the 5'
549 ends of predicted genes of interest using RNA-seq data and the information about predicted
550 signal peptides. The ATG codon preceding the signal peptide or the last ATG codon in the
551 second exon was designated as the putative start codon. As a general rule, the promoter
552 region included a sequence spanning from the 3' end of the closest upstream gene on the
553 same strand to the start codon, but if the upstream neighbor gene was located further than 2
554 kb away, a 1.5-2 kb region upstream of the identified start codon was designated as the
555 putative promoter. In the case of inverted tandem duplicates in the head-to-head orientation,
556 the 5' end of the promoter region was approximately in the middle between the start codons
557 of the two genes. For the reporter constructs, we used the previously published coding
558 sequences of TurboRFP[85] and Venus[27] fused with the 3' UTR of the ribosomal gene *rpl-23*[85].
559 For the *nhr-1* rescue construct, we used the native coding sequence, in which we replaced
560 native introns with synthetic introns, fused with the native 3' UTR. As the latter fragment could
561 not be amplified from genomic or complementary DNA in one piece, we purchased a
562 corresponding gBlocks fragments (Integrated DNA Technologies). FASTA sequences of all
563 promoter regions, coding sequences and 3' UTRs are provided in SData 1.

564 Plasmids carrying reporter and rescue constructs, listed in STable 2, were created by
565 Gibson assembly using NEBuilder HiFi DNA Assembly Master Mix (New England Biolabs) or
566 a homemade master mix[86]. Small modifications, such as deletions and insertions under 70 bp,
567 were introduced using Q5 Site-Directed Mutagenesis kit (New England Biolabs). Injection mix
568 for transformation was created by digesting the plasmid of interest, the marker plasmid
569 carrying a tail-bound reporter *egl-20p::TurboRFP* (if applicable), and genomic DNA with
570 FastDigest restriction enzymes (Thermo Fisher Scientific), whereby genomic DNA was cut
571 with an enzyme(s) that had the same cutting site(s) as the enzyme(s) used to digest the
572 plasmids. Digested DNA was purified using Wizard SV Gel and PCR Clean-Up system
573 (Promega), and the components were mixed in the following ratios. Injection mixes with rescue

574 constructs contained 1 ng/µL rescue construct, 10 ng/µL marker, and 50 ng/µL genomic DNA.
575 Injection mixes with reporter constructs contained 10 ng/µL reporter construct, 10 ng/µL
576 marker, and 60 ng/µL genomic DNA. The mix was injected in the gonad rachis of
577 approximately 1 day old hermaphrodites, and their progeny was screened for fluorescent
578 animals[85].
579
580 **Antibody staining**
581 We followed a previously published protocol[87] with minor modifications. Animals were
582 washed from mature plates with phosphate-buffered saline (PBS) (137 mM NaCl, 2.7 mM KCl,
583 10 mM Na_2HPO_4, 1.8 mM KH_2PO_4 at pH 7.4), passed over a 5-20 µm nylon filter, concentrated
584 at the bottom of a 2 mL tube and chilled on ice. We then added chilled fixative (15 mM Na-
585 PIPES at pH 7.4, 80 mM KCl, 20 mM NaCl, 10 mM Na_2EGTA, 5 mM Spermidine-HCl, 2%
586 paraformaldehyde, 40% MeOH), froze the worms in liquid nitrogen and thawed them on ice
587 for 1-2 h with occasional inversion. Subsequently, the animals were washed twice with Tris-
588 Triton buffer (100 mM Tris-HCl at pH 7.4, 1 mM EDTA, 1% Triton X-100), incubated in Tris-
589 Triton buffer with 1% β-mercaptoethanol in a thermomixer at 600 rpm for 2 h at 37°C, washed
590 once in borate buffer (25 mM H_3BO_3, 12.5 mM NaOH), incubated in borate buffer with 10 mM
591 dithiothreitol in a thermomixer at 600 rpm for 15 min at room temperature, washed once in
592 borate buffer, incubated in borate buffer with ~0.3% H_2O_2 in a thermomixer at 600 rpm for 15
593 min at room temperature, and washed once more in borate buffer. Next, the worms were
594 washed three times with antibody buffer B (0.1% bovine serum albumin, 0.5% Triton X-100,
595 0.05% NaN_3, 1 mM EDTA in PBS) on a rocking wheel, incubated with a dye-conjugated
596 antibody (Thermo Fisher Scientific, cat .# 26183-D550 and cat. # 26183-D488) diluted 1:25 in
597 antibody buffer A (1% bovine serum albumin, 0.5% Triton X-100, 0.05% NaN_3, 1 mM EDTA in
598 PBS) on a rocking wheel in the dark for 3 h at room temperature or overnight at 4°C, washed
599 three times with antibody buffer B and mounted on slides in a 1:1 mixture of PBS and
600 Vectashield (Vector Laboratories) with 1 µg/mL DAPI added. Slides were imaged using a Leica
601 SP8 confocal microscope.

RNA-seq analysis

To obtain a sufficient number of eggs, we passed young adult hermaphrodites to new agar plates with 5-10 animals per plate. After their F1 progeny have laid eggs (5-6 days), they were bleached (see above), then resuspended in 400 µL water per starting plate, pipetted onto multiple fresh plates with 100 µL suspension per fresh plate and placed at 20°C. Animals were collected at 24 h (corresponding to J2 and J3 larvae), 48 h (J3 and J4 larvae) and 68 h (J4 instar larvae and young adults) post-bleaching by adding some water to the plates, scraping off the bacterial lawns with worms in them using disposable cell spreaders and passing the resulting suspension through a 5 µm nylon filter, which efficiently separated worms from bacteria. Worms were washed from the filter into 1.5 mL tubes, pelleted in a table-top centrifuge at the maximum speed setting, after which the supernatant was removed and 1 mL TRIzol (Invitrogen) was added to the worm pellets. Tubes were flash-frozen in liquid nitrogen and stored at -80°C for up to a month. To extract RNA, worms suspended in TRIzol were frozen and thawed three times in liquid nitrogen, debris were pelleted for 10-15 min at 14,000 rpm at 4°C, and 200 µL of chloroform was added to the supernatant. After vigorous vortexing and incubation at room temperature (20-25°C) for 5 min, tubes were rotated for 15 min at 14,000 rpm at 4°C. The aqueous phase was combined with an equal volume of 100% ethanol, RNA was purified using RNA Clean & Concentrator Kit (Zymo Research) and its integrity was verified using RNA Nano chips on the Bioanalyzer 2100 instrument (Agilent). To analyze the transcriptome at the time of mouth form determination, we combined 500 ng RNA isolated at 24 h with 500 ng RNA isolated at 48 h post-bleaching, and proceeded to make libraries using NEBNext Ultra II Directional RNA Library Prep Kit for Illumina (New England Biolabs). To analyze the transcriptome at the time of mouth form differentiation, we prepared libraries from 1 µg of RNA isolated at 68 h post-bleaching. For wild type strain PS312, four biological replicates were collected at different time points. For the mutants, two replicates of two independent alleles were collected at two different time points, and these were treated as four biological replicates. Specifically, we sequenced the following alleles: *nhr-1(tu1163) loss-of-*

629 *function, nhr-1(tu1164) loss-of-function, nhr-40(tu505) gain-of-function, nhr-40(iub6) gain-of-*
630 *function, nhr-40(tu1418) loss-of-function, nhr-40(tu1423) null*.

631 Libraries were sequenced in two paired-end runs of a HiSeq 3000 machine, whereby
632 we aimed at 10-20 mln reads per library. Raw sequences have been deposited in the
633 European Nucleotide Archive with the study accession number PRJEB34615, and will be
634 made available upon acceptance. The fourth biological replicate of wild-type PS312 and all
635 replicates of the *nhr-40 loss-of-function/null* mutants were sequenced in a different run than
636 the other samples. To ensure that batch effects were negligible, we additionally re-sequenced
637 the first three replicates of wild-type PS312 in the same run and verified that coordinates in
638 PCA conducted using complete transcriptomes were minimally altered when comparing the
639 same samples sequenced in the two runs. Reads were mapped to the El Paco assembly of
640 the *P. pacificus* genome[78] using STAR (ver. 020201)[88]. Differential expression analysis was
641 carried out in R (ver. 3.4.4)[73] using Bioconductor (ver. 3.6)[89] and DESeq2 (ver. 1.18.1)[90],
642 whereby we counted reads mapping to El Paco v1 gene predictions[78]. We applied an adjusted
643 p-value cutoff of 0.05 and no fold change cutoff. Alignments and coverage were visualized in
644 IGV[80]. To examine the transcript levels of *nhr-1* and *nhr-40*, we repeated differential
645 expression analysis, whereby we counted reads mapping to Trinity-assembled transcripts
646 generated from previously published RNA-seq data[26] because the El Paco v1 gene prediction
647 for *nhr-1* was incorrect in that it was a fusion of multiple neighboring genes. To test the
648 differences in FPKM values for *nhr-1* and *nhr-40* in different mutants at each of the two time
649 points, we performed t-test as implemented in the t.test function in R (ver. 3.4.4)[73] and applied
650 false discovery rate (FDR) correction to the p-values obtained. Prior to conducting the t-test,
651 we verified the assumptions for parametric statistics by performing Shapiro-Wilk test for
652 normality (shapiro.test function) and Levene test for homoscedasticity (levene.test function of
653 the car package[91]). Signal peptides were predicted using SignalP (ver. 4.1)[92]. To compare
654 relative numbers of genes in different categories listed in Fig. 3B, we used chi-squared test as
655 implemented in the chisq.test function in R (ver. 3.4.4)[73].
656

Phylogenetic reconstructions

To identify NHR, CAP, and chitinase genes in the *C. elegans* genome, we retrieved the current version (PRJNA13758) of predicted proteins and domains from the http://wormbase.org website and selected genes that contained "IPR001628", "CAP domain", and "IPR001223" as predicted InterPro domains, respectively. The list of Astacin genes was taken from an earlier study[93] and the corresponding gene predictions were manually retrieved from the http://wormbase.org website. To identify NHR, Astacin, CAP, and chitinase genes in the *P. pacificus* genome, we predicted domains in the El Paco v1 version of gene predictions[78] using HMMER (ver. 3.1b2) software in conjunction with the PFAM profile database[94] and selected genes that contained "PF00105", "Astacin", "CAP", and "PF00704" as predicted PFAM domains, respectively. Manual inspection of the retrieved NHR genes in *P. pacificus* revealed that many of the gene predictions represent fusion of multiple neighboring genes. Therefore, we used the information about the predicted domains, RNA-seq data generated in this study, and Illumina and PacBio RNA-seq datasets generated earlier[26,95,96] to manually reannotate the NHR gene predictions in *P. pacificus*. We submitted the improved annotations to http://wormbase.org and they will be released in due course. For the tree of CAP domains in *P. pacificus* and *P. fissidentatus*, we predicted domains in the Pinocchio versions of gene predictions for both genomes[60] and selected genes that contained "PF00188" as a predicted PFAM domain. In the case of NHR genes, complete sequences were aligned, while in the case of other gene families, functional domains extracted using HMMER (ver. 3.1b2) were aligned to facilitate the alignment of genes with divergent domain architecture. Alignments were done in MAFFT (ver. 7.310)[97] and maximum likelihood trees were built using RAxML (ver. 8.2.11)[98]. Protein-based trees were generated with the following parameters: -f a -m PROTGAMMAAUTO -N 100. In the case of CAP domains in *P. pacificus* and *P. fissidentatus*, we first generated a protein-based tree and identified a poorly resolved subtree containing the genes of interest. To increase the number of informative sites, we extracted corresponding nucleotide sequences, aligned them in MAFFT and built a tree in RAxML with the following parameters: -f a -m GTRCAT -N 100. Obtained phylogenetic trees were visualized using

685 FigTree (ver. 1.4.2). All phylogenetic trees and corresponding alignments are provided in

686 SData 2.

687 ***References***

688 1. West-Eberhard, M. J. *Developmental plasticity and evolution*. (Oxford University Press,
689 2003).
690 2. Corona, M., Libbrecht, R. & Wheeler, D. E. Molecular mechanisms of phenotypic
691 plasticity in social insects. *Curr Opin Insect Sci* **13**, 55–60 (2016).
692 3. Nicotra, A. B. *et al.* Plant phenotypic plasticity in a changing climate. *Trends Plant Sci.*
693 **15**, 684–692 (2010).
694 4. Seebacher, F., White, C. R. & Franklin, C. E. Physiological plasticity increases
695 resilience of ectothermic animals to climate change. *Nat. Clim. Chang.* **5**, 61 (2014).
696 5. Charmantier, A. *et al.* Adaptive phenotypic plasticity in response to climate change in a
697 wild bird population. *Science* **320**, 800–803 (2008).
698 6. Oostra, V., Saastamoinen, M., Zwaan, B. J. & Wheat, C. W. Strong phenotypic plasticity
699 limits potential for evolutionary responses to climate change. *Nat. Commun.* **9**, 1005
700 (2018).
701 7. Susoy, V., Ragsdale, E. J., Kanzaki, N. & Sommer, R. J. Rapid diversification
702 associated with a macroevolutionary pulse of developmental plasticity. *Elife* **4**, e05463
703 (2015).
704 8. West-Eberhard, M. J. Developmental plasticity and the origin of species differences.
705 *Proc. Natl. Acad. Sci. U. S. A.* **102 Suppl 1**, 6543–6549 (2005).
706 9. Corl, A. *et al.* The Genetic Basis of Adaptation following Plastic Changes in Coloration in
707 a Novel Environment. *Curr. Biol.* **28**, 2970–2977.e7 (2018).
708 10. Wund, M. A., Baker, J. A., Clancy, B., Golub, J. L. & Foster, S. A. A test of the 'flexible
709 stem' model of evolution: ancestral plasticity, genetic accommodation, and
710 morphological divergence in the threespine stickleback radiation. *Am. Nat.* **172**, 449–
711 462 (2008).
712 11. Levis, N. A. & Pfennig, D. W. Phenotypic plasticity, canalization, and the origins of
713 novelty: Evidence and mechanisms from amphibians. *Semin. Cell Dev. Biol.* **88**, 80–90

(2019).

12. Ghalambor, C. K. *et al.* Non-adaptive plasticity potentiates rapid adaptive evolution of gene expression in nature. *Nature* **525**, 372–375 (2015).
13. Sommer, R. J. *et al.* The genetics of phenotypic plasticity in nematode feeding structures. *Open Biol.* **7**, 160332 (2017).
14. Projecto-Garcia, J., Biddle, J. F. & Ragsdale, E. J. Decoding the architecture and origins of mechanisms for developmental polyphenism. *Curr. Opin. Genet. Dev.* **47**, 1–8 (2017).
15. Opachaloemphan, C., Yan, H., Leibholz, A., Desplan, C. & Reinberg, D. Recent Advances in Behavioral (Epi)Genetics in Eusocial Insects. *Annu. Rev. Genet.* **52**, 489–510 (2018).
16. Moczek, A. P. *et al.* The role of developmental plasticity in evolutionary innovation. *Proc. Biol. Sci.* **278**, 2705–2713 (2011).
17. Bento, G., Ogawa, A. & Sommer, R. J. Co-option of the hormone-signalling module dafachronic acid-DAF-12 in nematode evolution. *Nature* **466**, 494–499 (2010).
18. Ragsdale, E. J., Müller, M. R., Rödelsperger, C. & Sommer, R. J. A Developmental Switch Coupled to the Evolution of Plasticity Acts through a Sulfatase. *Cell* **155**, 922–933 (2013).
19. Werner, M. S. *et al.* Environmental influence on *Pristionchus pacificus* mouth form through different culture methods. *Sci. Rep.* **7**, 7207 (2017).
20. Bose, N. *et al.* Complex small-molecule architectures regulate phenotypic plasticity in a nematode. *Angew. Chem. Int. Ed Engl.* **51**, 12438–12443 (2012).
21. Werner, M. S., Claaßen, M. H., Renahan, T., Dardiry, M. & Sommer, R. J. Adult Influence on Juvenile Phenotypes by Stage-Specific Pheromone Production. *iScience* **10**, 123–134 (2018).
22. Sieriebriennikov, B. *et al.* A Developmental Switch Generating Phenotypic Plasticity Is Part of a Conserved Multi-gene Locus. *Cell Rep.* **23**, 2835–2843.e4 (2018).
23. Namdeo, S. *et al.* Two independent sulfation processes regulate mouth-form plasticity in the nematode *Pristionchus pacificus*. *Development* **145**, dev166272 (2018).

24. Bui, L. T., Ivers, N. A. & Ragsdale, E. J. A sulfotransferase dosage-dependently regulates mouthpart polyphenism in the nematode Pristionchus pacificus. *Nat. Commun.* **9**, 4119 (2018).

25. Bui, L. T. & Ragsdale, E. J. Multiple plasticity regulators reveal targets specifying an induced predatory form in nematodes. *Molecular Biology and Evolution* (2019). doi:10.1093/molbev/msz171

26. Serobyan, V. *et al.* Chromatin remodelling and antisense-mediated up-regulation of the developmental switch gene *eud-1* control predatory feeding plasticity. *Nat. Commun.* **7**, 12337 (2016).

27. Kieninger, M. R. *et al.* The Nuclear Hormone Receptor NHR-40 Acts Downstream of the Sulfatase EUD-1 as Part of a Developmental Plasticity Switch in *Pristionchus*. *Curr. Biol.* **26**, 2174–2179 (2016).

28. Sluder, A. E., Mathews, S. W., Hough, D., Yin, V. P. & Maina, C. V. The nuclear receptor superfamily has undergone extensive proliferation and diversification in nematodes. *Genome Res.* **9**, 103–120 (1999).

29. Evans, R. M. & Mangelsdorf, D. J. Nuclear Receptors, RXR, and the Big Bang. *Cell* **157**, 255–266 (2014).

30. Brozová, E., Simecková, K., Kostrouch, Z., Rall, J. E. & Kostrouchová, M. NHR-40, a *Caenorhabditis elegans* supplementary nuclear receptor, regulates embryonic and early larval development. *Mech. Dev.* **123**, 689–701 (2006).

31. Crews, S. T. & Pearson, J. C. Transcriptional autoregulation in development. *Curr. Biol.* **19**, R241–6 (2009).

32. Mangan, S. & Alon, U. Structure and function of the feed-forward loop network motif. *Proc. Natl. Acad. Sci. U. S. A.* **100**, 11980–11985 (2003).

33. Macneil, L. T. & Walhout, A. J. M. Gene regulatory networks and the role of robustness and stochasticity in the control of gene expression. *Genome Res.* **21**, 645–657 (2011).

34. Bulcha, J. T. *et al.* A Persistence Detector for Metabolic Network Rewiring in an Animal. *Cell Rep.* **26**, 460–468.e4 (2019).

35. Abdusselamoglu, M. D., Eroglu, E., Burkard, T. R. & Knoblich, J. A. The transcription factor odd-paired regulates temporal identity in transit-amplifying neural progenitors via an incoherent feed-forward loop. *Elife* **8**, e46566 (2019).

36. Taylor-Teeples, M. *et al.* An *Arabidopsis* gene regulatory network for secondary cell wall synthesis. *Nature* **517**, 571–575 (2015).

37. Jaumouillé, E., Machado Almeida, P., Stähli, P., Koch, R. & Nagoshi, E. Transcriptional regulation via nuclear receptor crosstalk required for the *Drosophila* circadian clock. *Curr. Biol.* **25**, 1502–1508 (2015).

38. Anbalagan, M., Huderson, B., Murphy, L. & Rowan, B. G. Post-translational modifications of nuclear receptors and human disease. *Nucl. Recept. Signal.* **10**, e001 (2012).

39. Serobyan, V., Ragsdale, E. J., Müller, M. R. & Sommer, R. J. Feeding plasticity in the nematode *Pristionchus pacificus* is influenced by sex and social context and is linked to developmental speed. *Evol. Dev.* **15**, 161–170 (2013).

40. Hirschmann, H. Über das Vorkommen zweier Mundhöhlentypen bei *Diplogaster lheritieri* Maupas und *Diplogaster biformis* n. sp. und die Entstehung dieser hermaphroditischen Art aus *Diplogaster lheritieri*. *Zool. Jb., Abt. System., Ökol. u. Geogr* **80**, 132–170 (1951).

41. Reinke, V., Gil, I. S., Ward, S. & Kazmer, K. Genome-wide germline-enriched and sex-biased expression profiles in *Caenorhabditis elegans*. *Development* **131**, 311–323 (2004).

42. Gomis-Rüth, F. X., Trillo-Muyo, S. & Stöcker, W. Functional and structural insights into astacin metallopeptidases. *Biol. Chem.* **393**, 1027–1041 (2012).

43. Novelli, J., Ahmed, S. & Hodgkin, J. Gene interactions in *Caenorhabditis elegans* define DPY-31 as a candidate procollagen C-proteinase and SQT-3/ROL-4 as its predicted major target. *Genetics* **168**, 1259–1273 (2004).

44. Park, J.-O. *et al.* Characterization of the astacin family of metalloproteases in *C. elegans*. *BMC Dev. Biol.* **10**, 14 (2010).

45. Li, Y. *et al.* Structural insights into the interaction of the conserved mammalian proteins GAPR-1 and Beclin 1, a key autophagy protein. *Acta Crystallogr D Struct Biol* **73**, 775–792 (2017).
46. Darwiche, R., Kelleher, A., Hudspeth, E. M., Schneiter, R. & Asojo, O. A. Structural and functional characterization of the CAP domain of pathogen-related yeast 1 (Pry1) protein. *Sci. Rep.* **6**, 28838 (2016).
47. Choudhary, V. & Schneiter, R. Pathogen-Related Yeast (PRY) proteins and members of the CAP superfamily are secreted sterol-binding proteins. *Proc. Natl. Acad. Sci. U. S. A.* **109**, 16882–16887 (2012).
48. Gibbs, G. M., Roelants, K. & O'Bryan, M. K. The CAP superfamily: cysteine-rich secretory proteins, antigen 5, and pathogenesis-related 1 proteins - roles in reproduction, cancer, and immune defense. *Endocr. Rev.* **29**, 865–897 (2008).
49. Henrissat, B. *et al.* Conserved catalytic machinery and the prediction of a common fold for several families of glycosyl hydrolases. *Proc. Natl. Acad. Sci. U. S. A.* **92**, 7090–7094 (1995).
50. Lints, R. & Hall, D. H. The cuticle. in *WormAtlas* (2009).
51. Tokareva, O., Jacobsen, M., Buehler, M., Wong, J. & Kaplan, D. L. Structure-function-property-design interplay in biopolymers: spider silk. *Acta Biomater.* **10**, 1612–1626 (2014).
52. Guan, J., Vollrath, F. & Porter, D. Two mechanisms for supercontraction in *Nephila* spider dragline silk. *Biomacromolecules* **12**, 4030–4035 (2011).
53. Riebesell, M. & Sommer, R. J. Three-dimensional reconstruction of the pharyngeal gland cells in the predatory nematode *Pristionchus pacificus*. *Journal of Morphology* **278**, 1656–1666 (2017).
54. van Megen, H. *et al.* A phylogenetic tree of nematodes based on about 1200 full-length small subunit ribosomal DNA sequences. *Nematology* **11**, 927–950 (2009).
55. Altun, Z. F. & Hall, D. H. Alimentary System, Pharynx. in *WormAtlas* (2009).
56. Zhang, Y. C. & Baldwin, J. G. Ultrastructure of the postcorpus of the esophagus of

826 *Teratocephalus lirellus* (Teratocephalida) and its use for interpreting character evolution
827 in Secernentea (Nematoda). *Can. J. Zool.* **79**, 16–25 (2001).
828 57. Zhang Y. C. & Baldwin J. G. Ultrastructure of the post–corpus of *Zeldia punctata*
829 (Cephalobina) for analysis of the evolutionary framework of nematodes related to
830 *Caenorhabditis elegans* (Rhabditina). *Proceedings of the Royal Society of London.*
831 *Series B: Biological Sciences* **267**, 1229–1238 (2000).
832 58. Chiang, J.-T. A., Steciuk, M., Shtonda, B. & Avery, L. Evolution of pharyngeal behaviors
833 and neuronal functions in free-living soil nematodes. *J. Exp. Biol.* **209**, 1859–1873
834 (2006).
835 59. Zhang, Y. C. & Baldwin, J. G. Ultrastructure of the Esophagus of *Diplenteron* sp.
836 (Diplogasterida) to Test Hypotheses of Homology with Rhabditida and Tylenchida. *J.*
837 *Nematol.* **31**, 1–19 (1999).
838 60. Prabh, N. *et al.* Deep taxon sampling reveals the evolutionary dynamics of novel gene
839 families in *Pristionchus* nematodes. *Genome Res.* **28**, 1664–1674 (2018).
840 61. Dieterich, C. *et al.* The *Pristionchus pacificus* genome provides a unique perspective on
841 nematode lifestyle and parasitism. *Nat. Genet.* **40**, 1193–1198 (2008).
842 62. Markov, G. V., Baskaran, P. & Sommer, R. J. The same or not the same: lineage-
843 specific gene expansions and homology relationships in multigene families in
844 nematodes. *J. Mol. Evol.* **80**, 18–36 (2015).
845 63. Sieriebriennikov, B., Markov, G. V., Witte, H. & Sommer, R. J. The Role of DAF-
846 21/Hsp90 in Mouth-Form Plasticity in *Pristionchus pacificus*. *Mol. Biol. Evol.* **34**, 1644–
847 1653 (2017).
848 64. Antebi, A., Yeh, W. H., Tait, D., Hedgecock, E. M. & Riddle, D. L. *daf-12* encodes a
849 nuclear receptor that regulates the dauer diapause and developmental age in *C.*
850 *elegans*. *Genes Dev.* **14**, 1512–1527 (2000).
851 65. Burton, N. O. *et al.* Neurohormonal signaling via a sulfotransferase antagonizes insulin-
852 like signaling to regulate a *Caenorhabditis elegans* stress response. *Nat. Commun.* **9**,
853 5152 (2018).

66. Rödelsperger, C., Streit, A. & Sommer, R. J. Structure, Function and Evolution of The Nematode Genome. in *eLS* **26**, (John Wiley & Sons, Ltd, 2013).
67. Mitreva, M., Blaxter, M. L., Bird, D. M. & McCarter, J. P. Comparative genomics of nematodes. *Trends Genet.* **21**, 573–581 (2005).
68. Manning, G., Plowman, G. D., Hunter, T. & Sudarsanam, S. Evolution of protein kinase signaling from yeast to man. *Trends Biochem. Sci.* **27**, 514–520 (2002).
69. Goodrich, L. V., Johnson, R. L., Milenkovic, L., McMahon, J. A. & Scott, M. P. Conservation of the *hedgehog*/*patched* signaling pathway from flies to mice: induction of a mouse *patched* gene by Hedgehog. *Genes Dev.* **10**, 301–312 (1996).
70. Logan, C. Y. & Nusse, R. The Wnt signaling pathway in development and disease. *Annu. Rev. Cell Dev. Biol.* **20**, 781–810 (2004).
71. Stiernagle, T. Maintenance of *C. elegans* (February 11, 2006). in *WormBook* (ed. The C. elegans research community) (2016).
72. Schindelin, J. *et al.* Fiji: an open-source platform for biological-image analysis. *Nat. Methods* **9**, 676–682 (2012).
73. R Core Team. *R: A language and environment for statistical computing*. (R Foundation for Statistical Computing, 2016).
74. Adams, D. C. & Otarola-Castillo, E. geomorph: an R package for the collection and analysis of geometric morphometric shape data. *Methods Ecol. Evol.* **4**, 393–399 (2013).
75. Witte, H. *et al.* Gene inactivation using the CRISPR/Cas9 system in the nematode *Pristionchus pacificus*. *Dev. Genes Evol.* **225**, 55–62 (2015).
76. Lightfoot, J. W. *et al.* Small peptide-mediated self-recognition prevents cannibalism in predatory nematodes. *Science* **364**, 86–89 (2019).
77. Zhou, S. *et al.* Characterization of a non-sexual population of *Strongyloides stercoralis* with hybrid 18S rDNA haplotypes in Guangxi, Southern China. *PLoS Negl. Trop. Dis.* **13**, e0007396 (2019).
78. Rödelsperger, C. *et al.* Single-Molecule Sequencing Reveals the Chromosome-Scale

Genomic Architecture of the Nematode Model Organism *Pristionchus pacificus*. *Cell Rep.* **21**, 834–844 (2017).

79. Langmead, B. & Salzberg, S. L. Fast gapped-read alignment with Bowtie 2. *Nat. Methods* **9**, 357–359 (2012).
80. Robinson, J. T. *et al.* Integrative genomics viewer. *Nat. Biotechnol.* **29**, 24–26 (2011).
81. Pires-daSilva, A. *Pristionchus pacificus* protocols (March 14, 2013). in *WormBook* (ed. The C. elegans research community) (2013).
82. Li, H. & Durbin, R. Fast and accurate short read alignment with Burrows-Wheeler transform. *Bioinformatics* **25**, 1754–1760 (2009).
83. Li, H. *et al.* The Sequence Alignment/Map format and SAMtools. *Bioinformatics* **25**, 2078–2079 (2009).
84. Rae, R., Witte, H., Rödelsperger, C. & Sommer, R. J. The importance of being regular: *Caenorhabditis elegans* and *Pristionchus pacificus* defecation mutants are hypersusceptible to bacterial pathogens. *Int. J. Parasitol.* **42**, 747–753 (2012).
85. Schlager, B., Wang, X., Braach, G. & Sommer, R. J. Molecular cloning of a dominant roller mutant and establishment of DNA-mediated transformation in the nematode *Pristionchus pacificus*. *Genesis* **47**, 300–304 (2009).
86. OpenWetWare contributors. Gibson Assembly. *OpenWetWare* (2018). Available at: https://openwetware.org/mediawiki/index.php?title=Gibson_Assembly&oldid=1043969. (Accessed: 25th July 2018)
87. Bettinger, J. C., Lee, K. & Rougvie, A. E. Stage-specific accumulation of the terminal differentiation factor LIN-29 during *Caenorhabditis elegans* development. *Development* **122**, 2517–2527 (1996).
88. Dobin, A. *et al.* STAR: ultrafast universal RNA-seq aligner. *Bioinformatics* **29**, 15–21 (2013).
89. Gentleman, R. C. *et al.* Bioconductor: open software development for computational biology and bioinformatics. *Genome Biol.* **5**, R80 (2004).
90. Love, M. I., Huber, W. & Anders, S. Moderated estimation of fold change and dispersion

910 for RNA-seq data with DESeq2. *Genome Biol.* **15**, 550 (2014).

911 91. Fox, J. & Weisberg, S. An R Companion to Applied Regression. (2019).

912 92. Nielsen, H. Predicting Secretory Proteins with SignalP. *Methods Mol. Biol.* **1611**, 59–73

913 (2017).

914 93. Möhrlen, F., Hutter, H. & Zwilling, R. The astacin protein family in *Caenorhabditis*

915 *elegans*. *Eur. J. Biochem.* **270**, 4909–4920 (2003).

916 94. Finn, R. D. *et al.* The Pfam protein families database: towards a more sustainable

917 future. *Nucleic Acids Res.* **44**, D279–85 (2016).

918 95. Sinha, A., Langnick, C., Sommer, R. J. & Dieterich, C. Genome-wide analysis of trans-

919 splicing in the nematode *Pristionchus pacificus* unravels conserved gene functions for

920 germline and dauer development in divergent operons. *RNA* **20**, 1386–1397 (2014).

921 96. Werner, M. S. *et al.* Young genes have distinct gene structure, epigenetic profiles, and

922 transcriptional regulation. *Genome Res.* **28**, 1675–1687 (2018).

923 97. Katoh, K. & Standley, D. M. MAFFT multiple sequence alignment software version 7:

924 improvements in performance and usability. *Mol. Biol. Evol.* **30**, 772–780 (2013).

925 98. Stamatakis, A. RAxML version 8: a tool for phylogenetic analysis and post-analysis of

926 large phylogenies. *Bioinformatics* **30**, 1312–1313 (2014).

Acknowledgments

We are grateful to Gabi Eberhardt and Tobias Loschko for their assistance with the mutagenesis screens and Jürgen Berger for taking the SEM image of the *P. pacificus* mouth. We thank Dr. Michael Werner, Dr. Neel Prabh, Dr. Adrian Streit, and Metta Riebesell for the discussion. The study was funded by the Max Planck Society, and S.S. was supported by the China Scholarship Council.

Author contributions

B.S. designed and performed all experiments with help from other authors, analyzed the data, and wrote the manuscript together with R.J.S. and J.W.L.; S.S. designed and created reporter lines for Astacin genes, performed a suppressor screen in the *nhr-1* mutant background, and participated in mouth-form phenotyping; J.W.L. and E.M. generated *nhr-40* mutations using CRISPR/Cas9, J.W.L. additionally generated mutations in the downstream targets of NHR-1 and NHR-40 and wrote the manuscript together with B.S. and R.J.S.; C.R. performed bulk segregant analysis; H.W. generated CRISPR/Cas9 mutants and transgenes; R.J.S. designed and supervised the study, and wrote the manuscript together with B.S. and J.W.L.

Competing interests

The authors are not aware of any competing interests.

Materials & Correspondence

Correspondence and requests for materials should be addressed to R.J.S.

950 ***Figure legends***

951

952 **Fig. 1.** Mouth-form plasticity in *P. pacificus*. (**A**) Mouth structure of wild-type eurystomatous
953 (Eu) morph, wild-type stenostomatous (St) morph, *nhr-1* mutant, and *nhr-40* mutant.
954 Unlabeled images in two focal planes are shown in SFig. 1A. (**B**) Scanning electron
955 microscopy image of the mouth opening of the Eu morph. (**C**) The Eu morph devouring its
956 prey. (**D**) Putative gene regulatory network controlling mouth-form plasticity in *P. pacificus*.
957 (**E**) Design of the suppressor screen. D = dorsal, V= ventral, A = anterior, P = posterior, DT =
958 dorsal tooth, RVSLT = right ventrosublateral tooth, RVSLR = right ventrosublateral ridge,
959 EMS = ethyl methanesulfonate.

960

961 **Fig. 2.** Reverse genetics, transcriptomics and expression patterns of *nhr-40* and *nhr-1*. (**A**)
962 Protein structure of NHR-40 in wild-type and mutant animals. (**B**) Expression levels of *nhr-40*
963 and *nhr-1* in wild type and mutants as revealed by transcriptomic profiling. (**C**) Antibody
964 staining against the HA epitope in an *nhr-1* rescue line. (**D**) Expression patterns of *nhr-40*
965 and *nhr-1* transcriptional reporters in a double reporter line. TurboRFP (magenta) and Venus
966 (green) channels are presented as maximum intensity projections. Co-expression results in
967 white color. D = dorsal, V= ventral, A = anterior, P = posterior, N.S. = not significant.

968

969 **Fig. 3.** Target genes of NHR-40 and NHR-1. (**A**) Experimental setup of transcriptomics
970 experiment and selection criteria to identify target genes. (**B**) Trends among target genes
971 compared to genome-wide pattern. (**C**) Transmission electron microscopy reconstruction of
972 the dorsal pharyngeal gland cell (g1D) [53] and expression patterns of transcriptional reporters
973 for nine selected targets of NHR-40 and NHR-1. TurboRFP channel is presented as
974 standard deviation projections. *lof* = *loss-of-function*, *gof* = *gain-of-function*, *** = p<0.001, D
975 = dorsal, V= ventral, A = anterior, P = posterior.

976

977 **Fig. 4.** Evolution of pharynx morphology in the order Rhabditida.

978 **Fig. 5.** Evolution of *nhr-40*, *nhr-1*, and their target genes. Arrowheads point at the genes of
979 interest. Protein-based trees of NHR genes (**A**), Astacin domains (**B**), chitinase domains (**C**),
980 and CAP domains (**D**) in *P. pacificus* and *C. elegans*. (**E**) Nucleotide-based tree of the CAP
981 domains from a poorly-resolved protein-based subtree of all predicted CAP domains in *P.*
982 *pacificus* and *P. fissidentatus*.
983
984 **Table 1.** Mouth-form frequencies in wild type and mutant lines. The genotype of the
985 duodecuple Astacin mutant is *PPA03932(tu1259) PPA32730(tu1503);PPA05669(tu1316)*
986 *PPA05618(tu1317) PPA21987(tu1329) PPA16331(tu1339) PPA27985(tu1340)*
987 *PPA34430(tu1341) PPA20266(tu1385) PPA42924(tu1386);PPA05955(tu1481)*
988 *PPA42525(tu1482)*. The genotype of the quintuple CAP mutant is *tuDf6[PPA21912*
989 *PPA29522 PPA21910] tuDf7[PPA05611 PPA39470] tuDf8[PPA13058 PPA39735]*.
990
991 **Table 2.** List of targets of NHR-40 and NHR-1.

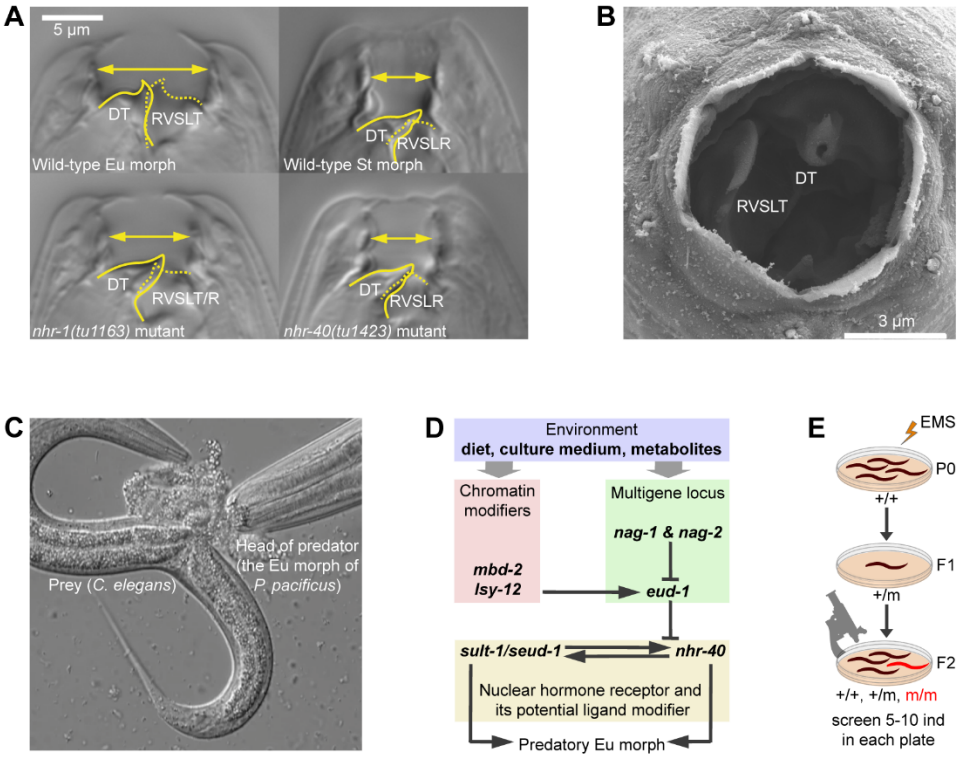

Fig. 1. Mouth-form plasticity in *P. pacificus*. (**A**) Mouth structure of wild-type eurystomatous (Eu) morph, wild-type stenostomatous (St) morph, *nhr-1* mutant, and *nhr-40* mutant. Unlabeled images in two focal planes are shown in SFig. 1A. (**B**) Scanning electron microscopy image of the mouth opening of the Eu morph. (**C**) The Eu morph devouring its prey. (**D**) Putative gene regulatory network controlling mouth-form plasticity in *P. pacificus*. (**E**) Design of the suppressor screen.
D = dorsal, V= ventral, A = anterior, P = posterior, DT = dorsal tooth, RVSLT = right ventrosublateral tooth, RVSLR = right ventrosublateral ridge, EMS = ethyl methanesulfonate.

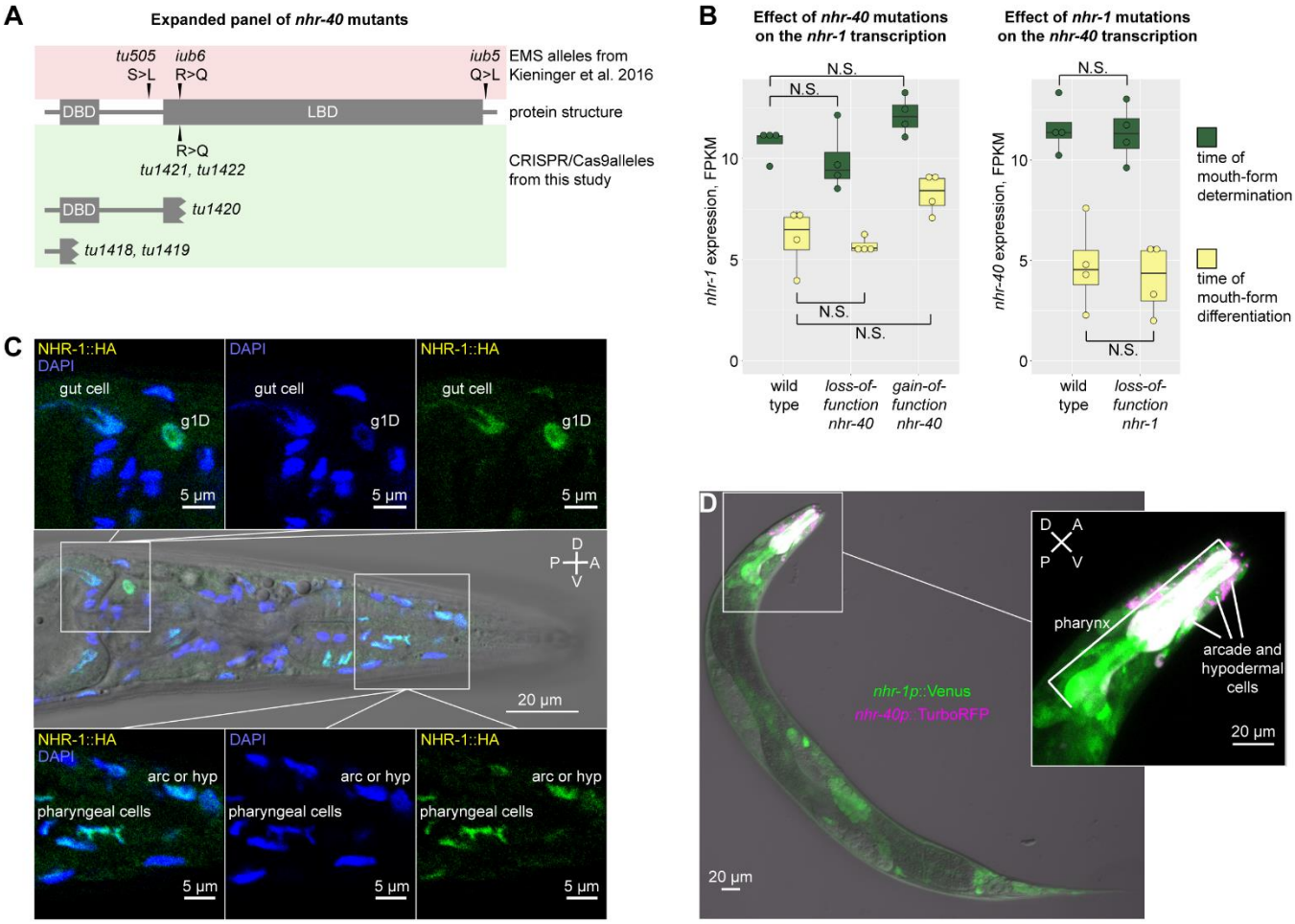

Fig. 2. Reverse genetics, transcriptomics and expression patterns of *nhr-40* and *nhr-1*. (**A**) Protein structure of NHR-40 in wild-type and mutant animals. (**B**) Expression levels of *nhr-40* and *nhr-1* in wild type and mutants as revealed by transcriptomic profiling. (**C**) Antibody staining against the HA epitope in an *nhr-1* rescue line. (**D**) Expression patterns of *nhr-40* and *nhr-1* transcriptional reporters in a double reporter line. TurboRFP (magenta) and Venus (green) channels are presented as maximum intensity projections. Co-expression results in white color.
D = dorsal, V= ventral, A = anterior, P = posterior, N.S. = not significant.

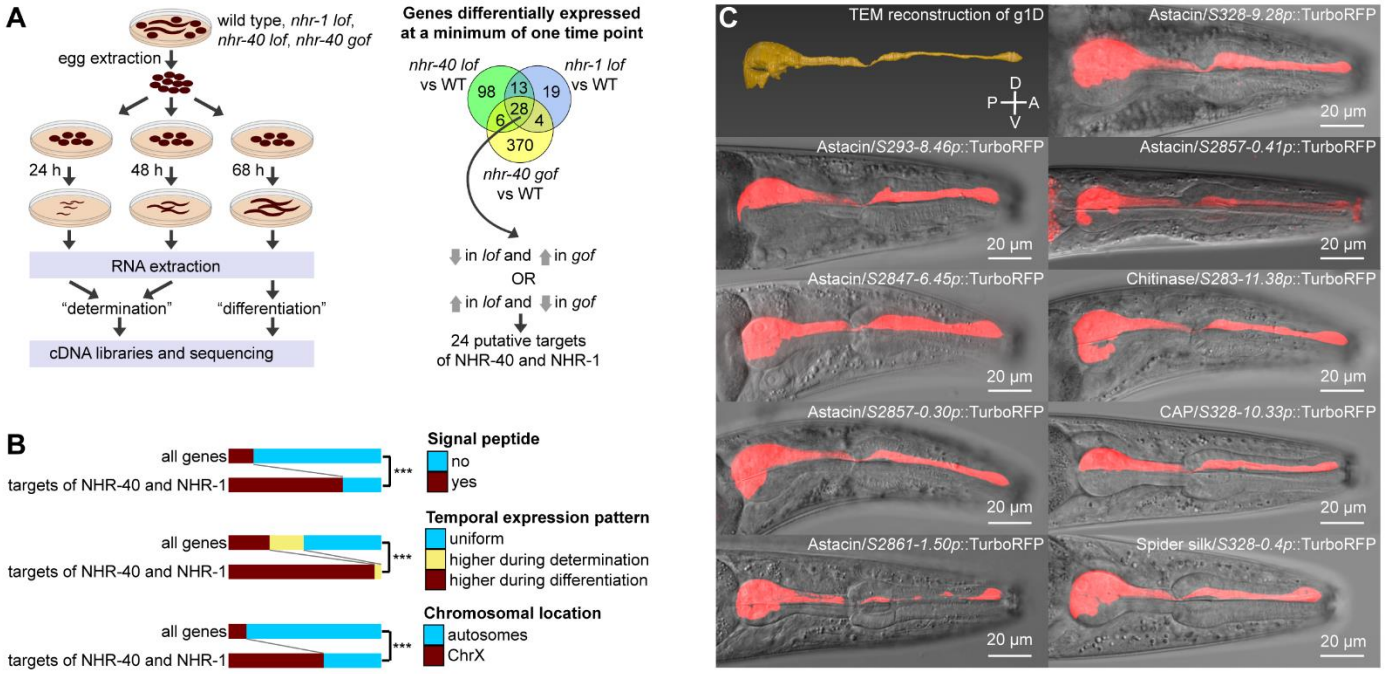

Fig. 3. Target genes of NHR-40 and NHR-1. (**A**) Experimental setup of transcriptomics experiment and selection criteria to identify target genes. (**B**) Trends among target genes compared to genome-wide pattern. (**C**) Transmission electron microscopy reconstruction of the dorsal pharyngeal gland cell (g1D) [52] and expression patterns of transcriptional reporters for nine selected targets of NHR-40 and NHR-1. TurboRFP channel is presented as standard deviation projections.
lof = loss of function, gof = gain of function, *** = p<0.001, D = dorsal, V= ventral, A = anterior, P = posterior.

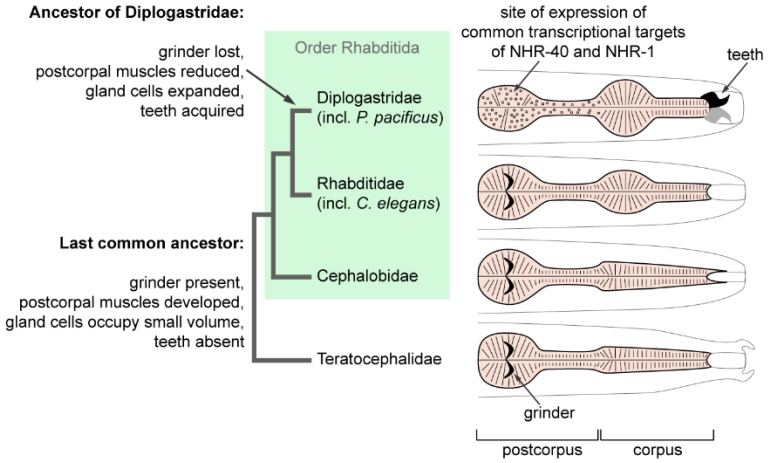

Fig. 4. Evolution of pharynx morphology in the order Rhabditida.

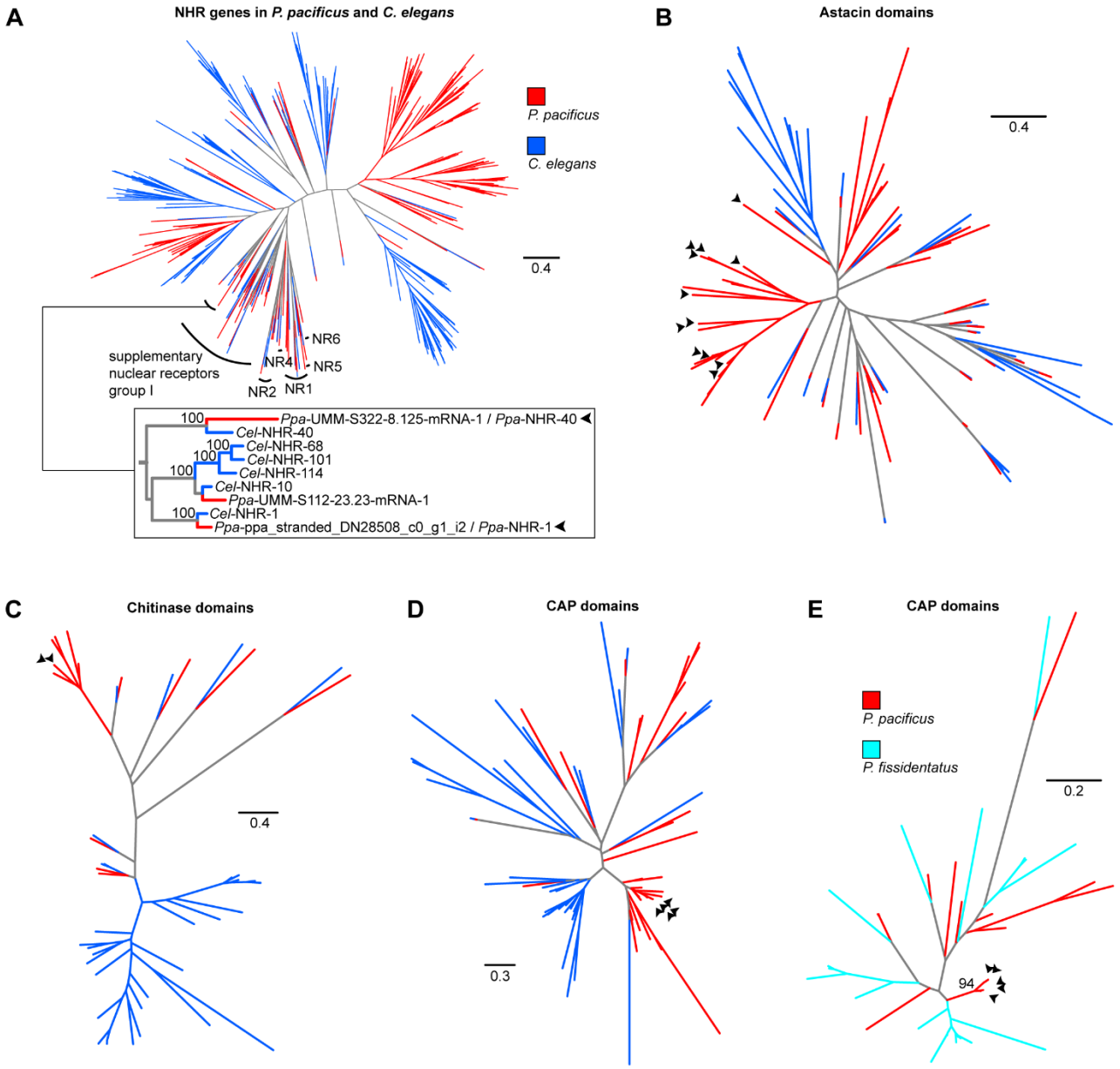

Fig. 5. Evolution of *nhr-40*, *nhr-1*, and their target genes. Arrowheads point at the genes of interest. Protein-based trees of NHR genes (**A**), Astacin domains (**B**), chitinase domains (**C**), and CAP domains (**D**) in *P. pacificus* and *C. elegans*. (**E**) Nucleotide-based tree of the CAP domains from a poorly-resolved protein-based subtree of all predicted CAP domains in *P. pacificus* and *P. fissidentatus*.

Table 1

Medium	Genotype	Eu, %	N
NGM agar	wild type PS312	98	650
NGM agar	*nhr-40(tu505)*	100	100
NGM agar	*nhr-40(tu505) tu515*	0	136
NGM agar	*tu515*	0	136
NGM agar	*nhr-1(tu1163)*	0	133
NGM agar	*nhr-1(tu1164)*	0	140
NGM agar	*nhr-1(tu1163)/tu515*	0	70
NGM agar	*nhr-1(tu1163);tuEx305[nhr-1(+);egl-20p::TurboRFP]*	85	110
NGM agar	*nhr-1(tu1163);tuEx310[nhr-1(+);egl-20p::TurboRFP]*	86	112
NGM agar	*nhr-1(tu1163);tuEx328[nhr-1(+)::HA;egl-20p::TurboRFP]*	86	150
NGM agar	*nhr-40(tu505) nhr-1(tu1163)*	2	134
NGM agar	*nhr-40(tu1418)*	0	150
NGM agar	*nhr-40(tu1419)*	0	150
NGM agar	*nhr-40(tu1420)*	0	150
NGM agar	*nhr-40(tu1423)*	0	150
NGM agar	*nhr-40(iub6)*	100	100
NGM agar	*nhr-40(tu1421)*	100	150
NGM agar	*nhr-40(tu1422)*	100	100
NGM agar	duodecuple Astacin mutant	98	55
NGM agar	quintuple CAP mutant	94	50
NGM agar	*PPA04200(tu1213) PPA39293(tu1214)*	100	50
NGM agar	*PPA04200(tu1216) PPA39293(tu1217)*	100	50
NGM agar	*PPA27560(tu1475)*	100	51
NGM agar	*PPA27560(tu1476)*	100	53
NGM agar	*PPA30108(tu1230)*	100	50
NGM agar	*PPA30108(tu1231)*	100	50
NGM agar	*PPA30435(tu1477)*	100	48
NGM agar	*PPA30435(tu1478)*	98	54
NGM agar	*PPA38892(tu1473)*	100	50
NGM agar	*PPA38892(tu1474)*	100	50
S-medium	wild type PS312	5	850
S-medium	*nhr-40(tu505)*	100	150
S-medium	*nhr-40(tu1418)*	0	150
S-medium	*nhr-40(tu1419)*	0	150
S-medium	*nhr-40(tu1420)*	0	150
S-medium	*nhr-40(tu1423)*	0	150
S-medium	*nhr-40(iub6)*	100	150
S-medium	*nhr-40(tu1421)*	100	150
S-medium	*nhr-40(tu1422)*	100	150

Table 2

Chromosome	Wormbase WS268 Identifier	El Paco annotation v1 Identifier	Predicted PFAM domains	Log fold change, *nhr-1* vs. wild type, determination time point	Log fold change, *nhr-1* vs. wild type, differentiation time point	Log fold change, *nhr-40 loss-of-function* vs. wild type, determination time point	Log fold change, *nhr-40 loss-of-function* vs. wild type, differentiation time point	Log fold change, *nhr-40 gain-of-function* vs. wild type, determination time point	Log fold change, *nhr-40 gain-of-function* vs. wild type, differentiation time point
ChrX	*PPA05669*	*UMM-S328-9.28-mRNA-1*	Astacin	-6.240745897	-7.986635198	-7.210987982	-7.830279165	2.097757153	1.095985392
ChrIV	*PPA42525*	*UMM-S2847-7.46-mRNA-1*	Astacin	-4.841545383	-4.002165721	-7.839896476	-4.679957866	1.436839716	not significant
ChrIV	*PPA05955*	*UMM-S2847-6.45-mRNA-1*	Astacin	-4.032019323	-3.717834286	-6.639723524	-5.984683399	1.574571506	1.061560179
ChrX	*PPA05618*	*UMM-S328-7.47-mRNA-1*	Astacin	-3.574438844	-2.916374055	-7.745129989	-7.021294279	1.499309832	0.981934683
ChrX	*PPA16331*	*UMA-S293-8.46-mRNA-1*	Astacin	-2.699652128	-4.119198644	-3.460891813	-4.200736918	1.709937147	not significant
ChrX	*PPA39735*	*UMM-S328-10.33-mRNA-1*	CAP	-2.204596416	-2.494207229	-5.147759463	-5.268476177	1.413344404	not significant
ChrI	*PPA32730*	*UMM-S57-4.91-mRNA-1*	Astacin	-2.196833674	-1.648291234	-3.691078865	-3.030762239	1.685906094	0.781158675
ChrX	*PPA13058*	*UMM-S328-10.78-mRNA-1*	CAP	-2.072130667	-2.430015473	-4.777644344	-4.798862505	1.417106528	not significant
ChrIV	*PPA39293*	*UMM-S283-11.38-mRNA-1*	Glyco_hydro_18	-1.78798789	-1.00008438	-2.965102834	-1.920988766	0.91017037	not significant
ChrX	*PPA29522*	*UMM-S322-3.5-mRNA-1*	CAP	-1.619243845	not significant	-3.144502729	-1.482861278	0.989651252	not significant
ChrX	*PPA39470*	*UMM-S293-11.30-mRNA-1*	CAP	-1.535650433	-2.217536886	-4.429166678	-4.946006302	1.368183938	not significant
ChrX	*PPA21910*	*UMA-S322-3.38-mRNA-1*	CAP	-1.360420618	not significant	-2.333203285	-1.220283993	0.933478914	not significant
ChrIV	*PPA04200*	*UMM-S283-11.45-mRNA-1*	Glyco_hydro_18; MFS_1	-1.260777947	-0.790389646	-2.139628634	-1.317889252	0.858388553	not significant
ChrX	*PPA21987*	*UMA-S322-7.39-mRNA-1*	Astacin	-1.088820963	-1.133945969	-1.538108635	not significant	0.872393205	0.857569687
ChrX	*PPA27985*	*UMS-S2861-1.50-mRNA-1*	Astacin	-1.024169798	-1.594336612	-1.391792366	-1.82457695	0.856234189	0.920390529
ChrX	*PPA30108*	*UMS-S328-0.4-mRNA-1*	none	-0.947256862	-1.972768009	-1.664145426	-3.055683539	1.366224893	0.725689297
ChrII	*PPA27560*	*UMS-S10-46.25-mRNA-1*	none	not significant	-2.543527944	not significant	-1.495616763	1.576247265	not significant
ChrI	*PPA30435*	*UMM-S57-36.5-mRNA-1*	Lectin_C	not significant	-2.47831085	-6.394747605	-7.477473473	1.742988559	0.834485758
ChrX	*PPA34430*	*UMA-S2861-1.27-mRNA-1*	Astacin	not significant	-2.034806495	-1.356487112	-2.16601043	0.954950699	0.920888012
ChrX	*PPA38892*	*UMM-S250-3.76-mRNA-1*	ShK	not significant	-1.978289093	-1.766665626	-2.237851004	0.974981875	not significant
ChrX	*PPA20266*	*UMM-S2857-0.30-mRNA-1*	Astacin	not significant	-1.886347752	-1.391984972	-2.526477858	1.083601827	not significant
ChrX	*PPA42924*	*UMM-S2857-0.41-mRNA-1*	Astacin	not significant	-1.144915897	not significant	-1.729607349	0.848434069	not significant
ChrI	*PPA03932*	*UMM-S7-5.16-mRNA-1*	Astacin	not significant	-1.111093666	not significant	-1.621750021	1.106139077	0.751674205
ChrIV	*PPA06264*	*UMA-S2838-46.74-mRNA-1*	adh_short; KR; THF_DHG_CYH_C	not significant	2.240401693	not significant	2.955986944	-2.049582222	not significant